

Turbulent drag reduction in magnetohydrodynamic and quasi-static magnetohydrodynamic turbulence

Mahendra K. Verma,^{1, a)} Shadab Alam,^{2, b)} and Soumyadeep Chatterjee^{1, c)}

¹⁾Department of Physics, Indian Institute of Technology, Kanpur, India 208016

²⁾Department of Mechanical Engineering, Indian Institute of Technology, Kanpur, India 208016

In hydrodynamic turbulence, the kinetic energy injected at large scales cascades to the inertial range, leading to a constant kinetic energy flux. In contrast, in magnetohydrodynamic (MHD) turbulence, a fraction of kinetic energy is transferred to the magnetic energy. Consequently, for the same kinetic energy injection rate, the kinetic energy flux in MHD turbulence is reduced compared to its hydrodynamic counterpart. This leads to relative weakening of the nonlinear term ($\langle |(\mathbf{u} \cdot \nabla)\mathbf{u}| \rangle$, where \mathbf{u} is the velocity field) and turbulent drag, but strengthening of the velocity field in MHD turbulence. We verify the above using shell model simulations of hydrodynamic and MHD turbulence. Quasi-static MHD turbulence too exhibits turbulent drag reduction similar to MHD turbulence.

I. INTRODUCTION

Frictional force in a turbulent flow is proportional to square of the flow velocity^{1,2}. This steep dependence of the frictional force or *turbulent drag* on the velocity makes it a major challenge in aerospace and automobile industry, as well as for flow engineering. Past experiments and numerical simulations report turbulent drag reduction in a dilute solution with polymers (see Tabor and de Gennes³, de Gennes⁴, Sreenivasan and White⁵, Benzi⁶, Benzi and Ching⁷, and references therein) and in solutions with bubbles and surfactants⁸. Despite many experimental and theoretical attempts, we are far from consensus on the mechanism behind this phenomenon. Researchers attribute the following factors for the drag reduction: viscoelasticity, nonlinear interactions between the polymer and the velocity field, interactions at the boundary layers, anisotropic stress, etc.³⁻⁷. Both, bulk and boundary layer dynamics may play a significant role in drag reduction. Yet, some researchers argue that the contributions from the bulk probably dominates that from the boundary layer⁵. In the present paper we study drag reduction in the bulk region of magnetohydrodynamics (MHD) and quasi-static magnetohydrodynamics (QSMHD) turbulence, but not for the bluff bodies in such flows.

In this paper, using the energy fluxes we show that MHD and QSMHD turbulence exhibit turbulent drag reduction. In particular, we demonstrate that an inclusion of magnetic field in a turbulent flow leads to reductions in kinetic energy cascade rate, the nonlinear term $\langle |(\mathbf{u} \cdot \nabla)\mathbf{u}| \rangle$ (where \mathbf{u} is the velocity field, and $\langle \cdot \rangle$ represents averaged value), and turbulent drag. In particular, we describe the turbulent drag reduction from the perspectives of energy transfers and energy flux in the bulk flow.

In a turbulent flow forced at large scales, the injected kinetic energy cascades to intermediate scale and then to small scales, where the energy flux is dissipated by viscous force. In pure hydrodynamic turbulence, the energy injection rate, kinetic energy flux, and the viscous dissipation are equal^{1,2,9,10}, and the turbulent drag is proportional to the kinetic energy flux. In MHD turbulence and QSMHD turbulence, a part of kinetic energy is converted to magnetic energy, as illustrated by a large body of works on energy transfer computations in MHD and QSMHD turbulence¹¹⁻¹⁸. The above energy transfers lead to a reduction in kinetic energy flux and the magnitude of the nonlinear term, and hence a reduction in turbulent drag in MHD and QSMHD turbulence.

Reduction in kinetic energy flux also takes place in polymeric turbulence and in bubbly turbulence. A common feature among these systems is that the kinetic energy is transferred to the elastic energy associated with the magnetic field, polymers, and bubbles. Here, magnetic field in MHD acts like a taut string; polymers as springs; and bubbles as elastic spheres. It is important to note that MHD turbulence is more complex than hydrodynamic turbulence^{2,19-21}.

To demonstrate the above we performed numerical simulations of shell models of hydrodynamic and MHD turbulence with identical kinetic energy injection rates. We observe that the kinetic energy flux and the nonlinear term $\langle |(\mathbf{u} \cdot \nabla)\mathbf{u}| \rangle$ for MHD turbulence are lower than the corresponding quantities for hydrodynamic turbulence, but the flow speeds for MHD turbulence is larger than that for hydrodynamic counterpart. We remark that turbulent drag reduction in MHD and QSMHD turbulence would be important for astrophysical and engineering applications. For example, magnetic field is imposed to suppress velocity fluctuations in crystal growth and plate rolling²²⁻²⁴. We will describe the applications to dynamo later in the paper.

The outline of the paper is as follows. In Sections II and III we relate turbulent drag reduction in hydrodynamic and hydromagnetic turbulence to energy fluxes. In Section IV we perform numerical simulations of hydro-

^{a)}Electronic mail: mkv@iitk.ac.in

^{b)}Electronic mail: shadab@iitk.ac.in

^{c)}Electronic mail: soumyade@iitk.ac.in

dynamic and MHD turbulence using shell models and verify that the turbulent drag is reduced in MHD turbulence. Sections V and VI cover drag reduction issues in QSMHD and polymeric turbulence respectively. We conclude in Sec. VII.

II. TURBULENT DRAG IN HYDRODYNAMIC TURBULENCE

In this section we briefly describe the energy flux in Kolmogorov's theory of hydrodynamic turbulence, and relate it to the turbulent drag. The equations for incompressible hydrodynamics are

$$\frac{\partial \mathbf{u}}{\partial t} + (\mathbf{u} \cdot \nabla) \mathbf{u} = -\nabla(p/\rho) + \nu \nabla^2 \mathbf{u} + \mathbf{F}_{\text{ext}}, \quad (1)$$

$$\nabla \cdot \mathbf{u} = 0, \quad (2)$$

where \mathbf{u}, p are respectively the velocity and pressure fields; ρ is the density which is assumed to be unity; ν is the kinematic viscosity; \mathbf{F}_{ext} is the external force employed at large scales that helps maintain a steady state.

The multiscale energy transfer and dynamics are conveniently described using Fourier modes. The external force \mathbf{F}_{ext} injects kinetic energy at large scales. For a wavenumber \mathbf{k} , the kinetic energy injection rate is

$$\mathcal{F}_{\text{ext}}(\mathbf{k}) = \Re[\mathbf{F}_{\text{ext}}(\mathbf{k}) \cdot \mathbf{u}^*(\mathbf{k})], \quad (3)$$

where \Re stands for the real part of the argument. We denote the total kinetic energy injection rate using ϵ_{inj} . That is,

$$\int_0^{k_f} d\mathbf{k} \mathcal{F}_{\text{ext}}(\mathbf{k}) \approx \epsilon_{\text{inj}}. \quad (4)$$

This injected kinetic energy cascades to larger wavenumbers as kinetic flux $\Pi_u(k)$. In the inertial range, $\Pi_u(k) = \epsilon_{\text{inj}}$ due to the absence of external force and negligible viscous dissipation^{1,2,9,25}.

This energy flux is dissipated in the dissipative range, and the total viscous dissipation rate is given by

$$\epsilon_u = \int d\mathbf{k} D_u(\mathbf{k}) = \int d\mathbf{k} 2\nu k^2 E_u(\mathbf{k}), \quad (5)$$

where

$$E_u(\mathbf{k}) = \frac{1}{2} |\mathbf{u}(\mathbf{k})|^2 \quad (6)$$

is modal kinetic energy, and

$$D_u(\mathbf{k}) = 2\nu k^2 E_u(\mathbf{k}) \quad (7)$$

is the modal viscous dissipation rate. Based on energetic arguments, we conclude that^{2,9,25}

$$\Pi_u(k) \approx \epsilon_{\text{inj}} \approx \epsilon_u \approx \frac{U^3}{d}, \quad (8)$$

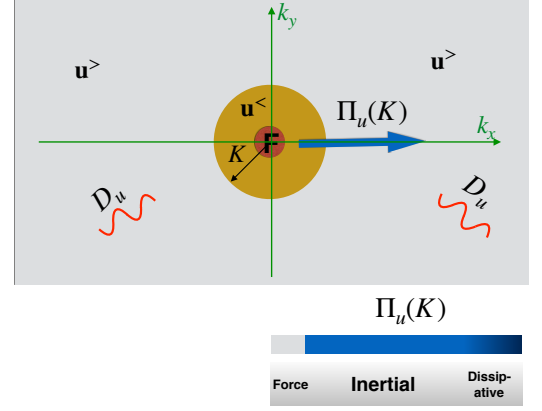


FIG. 1. (color online) In hydrodynamic turbulence, the energy supplied by the external force \mathbf{F}_{ext} at small wavenumbers (red sphere) cascades to the inertial range, leading to a constant kinetic energy flux $\Pi_u(k)$ in the inertial range. This flux is dissipated at small scales by viscosity. In the colorbar, the blue color represents constant $\Pi_u(k)$, while the black color represents depleted $\Pi_u(k)$.

where d is the large length scale of the system, and U is the large scale velocity. In this paper we take U as root mean square (rms) velocity. We illustrate the kinetic energy flux and the viscous dissipation in Fig. 1.

For the large scales, under a steady state, Eq. (1) yields the average turbulent drag $F_{D,\text{HD}}$ as

$$\langle F_{D,\text{HD}} \rangle_{\text{LS}} \approx \langle |(\mathbf{u} \cdot \nabla) \mathbf{u}| \rangle_{\text{LS}} \approx \langle F_{\text{ext}} \rangle, \quad (9)$$

where $\langle \cdot \rangle_{\text{LS}}$ represents ensemble averaging over the large scales. In terms of energy flux,

$$U F_{D,\text{HD}} \approx \Pi_u \approx \frac{U^3}{d} \approx \epsilon_{\text{inj}}, \quad (10)$$

or

$$F_{D,\text{HD}} \approx \frac{\Pi_u}{U} \approx \frac{U^2}{d}. \quad (11)$$

Note that the viscous dissipation can be ignored at large scales.

In the next section we will describe how the energy transfers from the velocity field to the magnetic field leads to a drag reduction in MHD turbulence.

III. DRAG REDUCTION IN MHD TURBULENCE IN TERMS OF ENERGY FLUX

The equations for incompressible MHD turbulence are

$$\frac{\partial \mathbf{u}}{\partial t} + (\mathbf{u} \cdot \nabla) \mathbf{u} = -\nabla(p/\rho) + \nu \nabla^2 \mathbf{u} + \mathbf{F}_u(\mathbf{B}, \mathbf{B}) + \mathbf{F}_{\text{ext}}, \quad (12)$$

$$\frac{\partial \mathbf{B}}{\partial t} + (\mathbf{u} \cdot \nabla) \mathbf{B} = \eta \nabla^2 \mathbf{B} + \mathbf{F}_B(\mathbf{B}, \mathbf{u}), \quad (13)$$

$$\nabla \cdot \mathbf{u} = 0, \quad (14)$$

$$\nabla \cdot \mathbf{B} = 0, \quad (15)$$

where \mathbf{u}, \mathbf{B} are respectively the velocity and magnetic fields; p is the total (thermal + magnetic) pressure, ρ is the density which is assumed to be unity; ν is the kinematic viscosity; η is the magnetic diffusivity; \mathbf{F}_{ext} is the external force employed at large scales; and

$$\mathbf{F}_u = (\mathbf{B} \cdot \nabla) \mathbf{B}, \quad (16)$$

$$\mathbf{F}_B = (\mathbf{B} \cdot \nabla) \mathbf{u} \quad (17)$$

represent respectively the Lorentz force and the stretching of the magnetic field by the velocity field. Such interactions lead to energy exchanges among the field variables. In the above equations, the magnetic field \mathbf{B} is in units of velocity, which is achieved by using $\mathbf{B} = \mathbf{B}_{\text{cgs}}/\sqrt{4\pi\rho}$. Here, \mathbf{B}_{cgs} is the magnetic field in CGS units.

Computation of multiscale energy transfers are quite convenient in spectral or Fourier space, in which the evolution equation for the modal kinetic energy $E_u(\mathbf{k}) = |\mathbf{u}(\mathbf{k})|^2/2$ is^{1,2,25–28}

$$\frac{d}{dt} E_u(\mathbf{k}) = T_u(\mathbf{k}) + \mathcal{F}_u(\mathbf{k}) + \mathcal{F}_{\text{ext}}(\mathbf{k}) - D_u(\mathbf{k}), \quad (18)$$

where

$$T_u(\mathbf{k}) = \sum_{\mathbf{p}} \Im [\{\mathbf{k} \cdot \mathbf{u}(\mathbf{q})\} \{\mathbf{u}(\mathbf{p}) \cdot \mathbf{u}^*(\mathbf{k})\}], \quad (19)$$

$$\begin{aligned} \mathcal{F}_u(\mathbf{k}) &= \Re [\mathbf{F}_u(\mathbf{k}) \cdot \mathbf{u}^*(\mathbf{k})] \\ &= \sum_{\mathbf{p}} -\Im [\{\mathbf{k} \cdot \mathbf{B}(\mathbf{q})\} \{\mathbf{B}(\mathbf{p}) \cdot \mathbf{u}^*(\mathbf{k})\}] \end{aligned} \quad (20)$$

with \Re, \Im representing the real and imaginary parts respectively, and $\mathbf{q} = \mathbf{k} - \mathbf{p}$. Note that $\mathcal{F}_{\text{ext}}(\mathbf{k})$ and $D_u(\mathbf{k})$ have been defined in Eqs. (3) and (7) respectively. In this paper we do not discuss the energetics of \mathbf{B} field because the turbulent drag reduction is related to the energy fluxes associated with the velocity field. When we sum Eq. (18) over all the modes in the wavenumber sphere of radius K , we obtain the following equation^{1,2,28}:

$$\begin{aligned} \frac{d}{dt} \sum_{k \leq K} E_u(\mathbf{k}) &= \sum_{k \leq K} T_u(\mathbf{k}) + \sum_{k \leq K} \mathcal{F}_u(\mathbf{k}) \\ &\quad + \sum_{k \leq K} \mathcal{F}_{\text{ext}}(\mathbf{k}) - \sum_{k \leq K} D_u(\mathbf{k}). \end{aligned} \quad (21)$$

The first term $\sum_{k \leq K} T_u(\mathbf{k})$ is the net energy transfer from the modes outside the sphere to the modes inside the sphere due to the nonlinear term $(\mathbf{u} \cdot \nabla) \mathbf{u}$. It is also negative of the kinetic energy flux for the sphere because

$$\Pi_u(K) = - \sum_{k \leq K} T_u(\mathbf{k}). \quad (22)$$

The second term $\sum_{k \leq K} \mathcal{F}_u(\mathbf{k})$ represents the total energy transfer rate to the velocity modes inside the sphere from all the magnetic modes^{12,27}. Since

$$\Pi_B(K) = - \sum_{k \leq K} \mathcal{F}_u(\mathbf{k}), \quad (23)$$

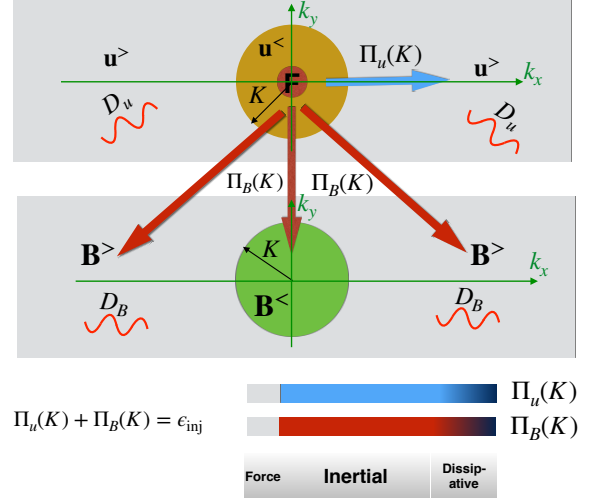


FIG. 2. (color online) In MHD turbulence, a fraction of kinetic energy flux is transferred to the magnetic field. $\Pi_u(K)$ is the kinetic energy flux for the velocity wavenumber sphere of radius K (yellow sphere), and $\Pi_B(K)$ is the net energy transfer from \mathbf{u} modes inside the sphere to all the \mathbf{B} modes. The external force injects kinetic energy into the small red sphere with the rate of ϵ_{inj} . The energy fluxes are dissipated with the dissipation rates D_u and D_B . In the inertial range, $\Pi_u(K) + \Pi_B(K) \approx \epsilon_{\text{inj}}$. In the colorbars, the light-blue color represents a constant kinetic energy flux $\Pi_u(k)$, while the red color represents $\Pi_B(K)$. The black color in the dissipation range represents depleted fluxes. Light-blue colored $\Pi_u(k)$ for MHD turbulence is lower than corresponding dark-blue colored $\Pi_u(k)$ for hydrodynamic turbulence.

the second term is negative of the net energy flux from the velocity modes inside the sphere to all the magnetic modes. The third term $\sum_{k \leq K} \mathcal{F}_{\text{ext}}(\mathbf{k})$ is the net energy injected by the external force \mathbf{F}_{ext} (represented by the red sphere of Fig. 2). The last term $\sum_{k \leq K} D_u(\mathbf{k})$ is the total viscous dissipation rate inside the sphere. See Figure 2 for an illustration of the above quantities.

For a wavenumber sphere of radius K , under a steady state ($d \sum_{k \leq K} E_u(\mathbf{k})/dt = 0$), the kinetic energy injected by \mathbf{F}_{ext} is lost to the two fluxes (Π_u, Π_B) and the total viscous dissipation rate. That is,

$$\Pi_u(K) + \Pi_B(K) + \sum_{k \leq K} D_u(\mathbf{k}) = \epsilon_{\text{inj}}. \quad (24)$$

In the inertial range where $D_u(\mathbf{k}) \approx 0$, we obtain

$$\Pi_u(K) + \Pi_B(K) \approx \epsilon_{\text{inj}}. \quad (25)$$

Following similar lines of arguments as in the previous section, we estimate the turbulent drag in MHD turbulence using

$$\langle F_{D,\text{MHD}} \rangle \approx \langle |(\mathbf{u} \cdot \nabla) \mathbf{u}| \rangle_{\text{LS}} \approx \frac{\Pi_u}{U}. \quad (26)$$

Using Eq. (25) we deduce that

$$\langle F_{D,\text{MHD}} \rangle \approx \frac{\epsilon_{\text{inj}} - \Pi_B}{U}. \quad (27)$$

Researchers have studied the energy fluxes Π_u and Π_B in detail for various combinations of parameters—forcing functions, boundary condition, ν and η (or their ratio $\text{Pm} = \nu/\eta$, which is called the *magnetic Prandtl number*). For example, Mininni et al.²⁹ computed the fluxes Π_u and Π_B using numerical simulations, and observed that $\Pi_B > 0$, and hence

$$\Pi_{u,\text{MHD}} < \Pi_{u,\text{HD}}. \quad (28)$$

That is, the kinetic energy flux in MHD turbulence is lower than the corresponding flux in hydrodynamic turbulence (without magnetic field). Using numerical simulations, Debliquy et al.¹⁵, Kumar et al.¹⁶, Verma and Kumar³⁰ arrived at a similar conclusion. In particular, using a shell model, Verma and Kumar³⁰ simulated MHD turbulence for $\text{Pm} = 1$ and showed that in the inertial range, $\Pi_u \approx 0.06 \pm 0.02$ and $\Pi_B \approx 0.93 \pm 0.02$; this result indicates a drastic reduction of kinetic energy flux in MHD turbulence. Note that, Π_B , the energy transferred from the velocity field to the magnetic field is responsible for the enhancement of magnetic field in astrophysical dynamos (e.g., in planets, stars, and galaxies)³¹. Laboratory experiments (see Monchaux *et al.*³² and references therein) too exhibit similar energy transfers. Based on these observations on the energy fluxes, we deduce that

$$F_{D,\text{MHD}} < F_{D,\text{HD}}, \quad (29)$$

or turbulent drag is reduced in MHD turbulence. Quantitatively, it will be more appropriate to compute drag-reduction coefficients:

$$c_1 = \frac{\Pi_u}{U^3/d}; \quad c_2 = \frac{\langle |(\mathbf{u} \cdot \nabla) \mathbf{u}| \rangle}{U^2/d}. \quad (30)$$

Note that $c_1, c_2 \approx 1$ for hydrodynamic turbulence, and they are expected to be lower than unity for MHD turbulence.

The aforementioned reduction in the energy flux and the nonlinear term $\langle |(\mathbf{u} \cdot \nabla) \mathbf{u}| \rangle$ lead to stronger large-scale velocity (U) in MHD turbulence than in the corresponding hydrodynamic turbulence. Note that strong and coherent U yields a diminished $\langle |(\mathbf{u} \cdot \nabla) \mathbf{u}| \rangle$ and kinetic energy flux. This is because the kinetic energy flux depends on U as well as on the phase relations between the velocity Fourier modes^{26,27}. We illustrate the above based on the numerical simulations of Yadav *et al.*³³. They showed that in a subcritical dynamo transition, U increases abruptly when the magnetic field becomes nonzero at the onset of dynamo (see Fig. 4 of Yadav *et al.*³³). Note that in the dynamo simulations of Yadav *et al.*³³, the flow exhibits turbulent behaviour even though the Reynolds number is not very large. Hence, the energy fluxes are expected to be significant in these

situations. Contrast these features with those in laminar regime in which the the Lorentz force increases the drag.

Though the past results on energy fluxes provide strong credence towards drag reduction in MHD turbulence, we need a clear-cut demonstration of the same. Towards this objective, we performed simulations of shell models for hydrodynamic and MHD turbulence with same kinetic energy injection rates. We show that the the kinetic energy flux and $\langle |(\mathbf{u} \cdot \nabla) \mathbf{u}| \rangle$ are reduced for MHD turbulence, but U for MHD turbulence is larger than that for hydrodynamic turbulence. We will report these results in the next section.

IV. NUMERICAL VERIFICATION USING SHELL MODEL

We employ a well-known Gledzer-Ohkitani-Yamada (GOY) shell model^{34,35} of hydrodynamic and MHD turbulence to quantify the kinetic energy flux, root mean square (rms) velocity, and nonlinear term connected to $(\mathbf{u} \cdot \nabla) \mathbf{u}$ discussed in previous sections. Based on these quantities we will show that the turbulent drag is indeed reduced in MHD turbulence compared to hydrodynamic turbulence.

The equation for the GOY shell model for hydrodynamic turbulence is

$$\frac{du_n}{dt} = N_n[u, u] - \nu k_n^2 u_n + F_{\text{ext},n}, \quad (31)$$

where u_n and $F_{\text{ext},n}$ represent respectively the velocity and external force fields for shell n , $k_n = k_0 \lambda^n$ is the wavenumber of the n th shell, and ν is the kinematic viscosity. Note that λ is a constant, and it is taken to be golden ratio³⁶. The mathematical expression of $N_n[u, u]$ is

$$N_n[u, u] = -i(a_1 k_n u_{n+1}^* u_{n+2}^* + a_2 k_{n-1} u_{n+1}^* u_{n-1}^* + a_3 k_{n-2} u_{n-1}^* u_{n-2}^*), \quad (32)$$

where a_1, a_2 and a_3 are constants. The conservation of kinetic energy ($\int d\mathbf{r} (u^2/2)$) and kinetic helicity ($\int d\mathbf{r} (\mathbf{u} \cdot \boldsymbol{\omega})$, where $\boldsymbol{\omega}$ denotes vorticity field) for force-less and dissipationless regime helps us determine the values of constant a_1, a_2, a_3 . A choice of the constants used in previous simulations and also in this paper are $a_1 = \lambda$, $a_2 = 1 - \lambda$ and $a_3 = -1$.

There are many shell models for MHD turbulence, e.g., see^{37–39}. However, in this paper we employ the GOY-based shell model proposed by Verma and Kumar³⁰, which is

$$\frac{du_n}{dt} = N_n[u, u] + M_n[B, B] - \nu k_n^2 u_n + F_{\text{ext},n}, \quad (33)$$

$$\frac{dB_n}{dt} = O_n[u, B] + P_n[B, u] - \eta k_n^2 B_n, \quad (34)$$

where B_n is the shell variable for the magnetic field, and η is the magnetic diffusivity. In addition to $N_n[u, u]$

of Eq. (32), there are three additional nonlinear terms $M_n[B, B]$, $O_n[u, B]$ and $P_n[B, u]$, which are

$$M_n[B, B] = -2i(b_1 k_n B_{n+1}^* B_{n+2}^* + b_2 k_{n-1} B_{n+1}^* B_{n-1}^* + b_3 k_{n-2} B_{n-1}^* B_{n-2}^*), \quad (35)$$

$$O_n[u, B] = -i[k_n(d_1 u_{n+1}^* B_{n+2}^* + d_3 B_{n+1}^* u_{n+2}^*) + k_{n-1}(-d_3 u_{n+1}^* B_{n-1}^* + d_2 B_{n+1}^* u_{n-1}^*) - k_{n-2}(d_1 u_{n-1}^* B_{n-2}^* + d_2 B_{n-1}^* u_{n-2}^*)], \quad (36)$$

$$P_n[B, u] = i[k_n(b_2 u_{n+1}^* B_{n+2}^* + b_3 B_{n+1}^* u_{n+2}^*) + k_{n-1}(b_3 u_{n+1}^* B_{n-1}^* + b_1 B_{n+1}^* u_{n-1}^*) + k_{n-2}(b_2 u_{n-1}^* B_{n-2}^* + b_1 B_{n-1}^* u_{n-2}^*)], \quad (37)$$

where $\{b_1, b_2, b_3\}$ and $\{d_1, d_2, d_3\}$ are the constants. Akin to hydrodynamic turbulence, these constants are computed using the conservation of the total energy ($\int d\mathbf{r}(u^2 + B^2)/2$), the magnetic helicity ($\int d\mathbf{r}(\mathbf{A} \cdot \mathbf{B})$, where \mathbf{A} is magnetic vector potential) and the cross helicity ($\int d\mathbf{r}(\mathbf{u} \cdot \mathbf{B})$) for $\nu = \eta = 0$ and $F_{\text{ext},n} = 0$. It is also ensured that the pure fluid case ($B_n = 0$) satisfies the conservation of kinetic energy and kinetic helicity. These constraints yield the following values of the constants³⁰:

$$b_1 = \lambda, b_2 = 1 + \frac{\lambda}{2}, b_3 = -1 - \frac{3\lambda}{2}, \quad (38)$$

$$d_1 = \frac{5\lambda}{2}, d_2 = -\lambda + 2, d_3 = -\frac{\lambda}{2}. \quad (39)$$

Note that the expression of $N_n[u, u]$ and the constants a_1 , a_2 , and a_3 are same as those for hydrodynamic turbulence discussed earlier.

We simulate the shell models for hydrodynamic and MHD turbulence for identical kinetic energy injection rate, and compare the kinetic energy fluxes, $\langle |(\mathbf{u} \cdot \nabla) \mathbf{u}| \rangle$, and the rms velocities for the two models. For the simulations, we divide wavenumbers into 36 logarithmically binned shells and take $\lambda = (\sqrt{5} + 1)/2$, the golden ratio. For time integration, we use Runge-Kutta fourth order (RK4) scheme with a fixed Δt . We carry out our hydrodynamic and MHD simulation up to 1000 eddy turnover time unit.

As illustrated in Figures 1 and 2, we force the large-scale velocity field using external random force at shells $n = 1$ and 2 such that the kinetic energy supply rate is maintained at a constant value. For the same, we employ the scheme proposed by Stepanov and Plunian³⁸. We perform three sets of simulations with kinetic energy supply rates $\epsilon_{\text{inj}} = 0.1, 1.0$ and 10.0 , and $\nu, \eta = 10^{-6}$. For $\epsilon_{\text{inj}} = 0.1$ and 1.0 , we choose $\Delta t = 5 \times 10^{-5}$, but for $\epsilon_{\text{inj}} = 10.0$, we take $\Delta t = 10^{-5}$. The numerical results are summarized in Table I.

The simulations reach their respective steady states after around 200 eddy turn over times. In Figure 3, for the steady states, we plot the time series of the kinetic energy for hydrodynamic simulations; and kinetic, magnetic, and total energies for MHD simulations for the three injection rates. The time series demonstrate that for the same ϵ_{inj} , the kinetic energy for MHD turbulence

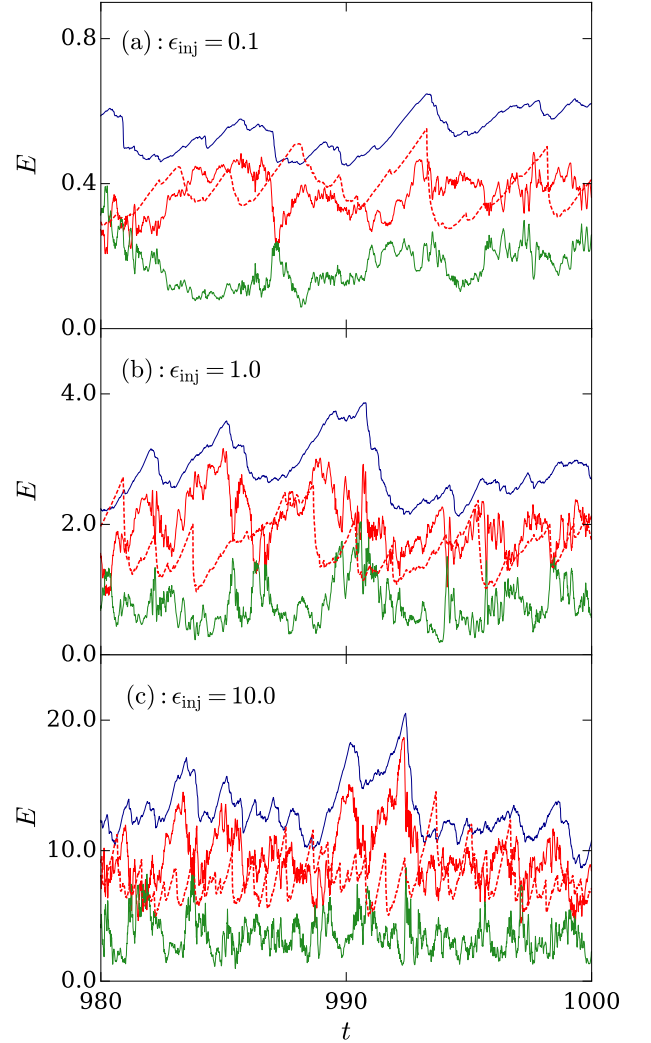


FIG. 3. (color online) Time evolution plots of the kinetic energy for hydrodynamics (red dashed curves), as well as those of the kinetic energy (solid red curves), magnetic energy (green curves), and total energy (dark-blue curves) for MHD turbulence. The three subplots represent the results for injection rates (a) $\epsilon_{\text{inj}} = 0.1$, (b) $\epsilon_{\text{inj}} = 1.0$, and (c) $\epsilon_{\text{inj}} = 10.0$.

is typically larger than that for the hydrodynamic turbulence. These observations clearly demonstrate an enhancement of the speed in MHD turbulence than hydrodynamic turbulence, as described in Sec. III.

For hydrodynamic and MHD turbulence, using the numerical u_n from the shell models, we estimate the rms value of the velocity using

$$U = \left\langle \sum_n |u_n|^2 \right\rangle^{1/2}, \quad (40)$$

TABLE I. For the three sets of shell model simulations of hydrodynamic and MHD turbulence with kinetic energy injection rates $\epsilon_{\text{inj}} = 0.1, 1.0$ and 10.0 , the table contains the numerical values of kinetic energy flux (Π_u) in the inertial range; rms velocity (U); and $\langle |(\mathbf{u} \cdot \nabla) \mathbf{u}| \rangle = \langle \sum_n |N_n[u, u]|^2 \rangle^{1/2}$.

	Hydrodynamics			MHD		
ϵ_{inj}	Π_u	U	$\langle (\mathbf{u} \cdot \nabla) \mathbf{u} \rangle$	Π_u	U	$\langle (\mathbf{u} \cdot \nabla) \mathbf{u} \rangle$
0.1	0.1	0.87	8.77	0.02	0.92	4.17
1.0	1.0	1.88	47.48	0.21	2.02	23.79
10.0	10.0	3.95	271.88	2.06	4.33	136.44

and the rms values of $(\mathbf{u} \cdot \nabla) \mathbf{u}$ using the formula:

$$\langle |(\mathbf{u} \cdot \nabla) \mathbf{u}| \rangle = \left\langle \sum_n |N_n[u, u]|^2 \right\rangle^{1/2}. \quad (41)$$

We average the computed values over 50000 frames during the steady state. These values are further averaged over 16 different simulations that were started with random initial condition. The results listed in Table I indicate a relative suppression of $\langle |(\mathbf{u} \cdot \nabla) \mathbf{u}| \rangle$ in MHD turbulence compared to hydrodynamic turbulence. However

$$U_{\text{MHD}} > U_{\text{HD}} \quad (42)$$

indicating a relative enhancement of the velocity in MHD turbulence. Note that the $\langle |(\mathbf{u} \cdot \nabla) \mathbf{u}| \rangle$ depends critically on the phases of the Fourier modes; larger U does not necessarily imply larger $\langle |(\mathbf{u} \cdot \nabla) \mathbf{u}| \rangle$.

Using the numerical data, we also compute the averaged kinetic energy spectrum

$$E_u(k) = \frac{1}{2k_n} \langle u_n^2 \rangle \quad (43)$$

for hydrodynamic and MHD turbulence. We adopt the same averaging procedure as done for the computation of U and $\langle |(\mathbf{u} \cdot \nabla) \mathbf{u}| \rangle$. The energy spectra exhibited in Figure 4 for the three sets show $k^{-5/3}$ power law in the inertial range. For each case, $E_u(k)$ for hydrodynamic and MHD turbulence are almost equal to each other, except at small and large wavenumbers. At small wavenumbers $E_u(k)$ for MHD turbulence is larger than that for hydrodynamics, consistent with the observation that $U_{\text{MHD}} > U_{\text{HD}}$. Also, note that the trend is reversed at large wavenumbers, whose role in turbulent drag reduction needs to be explored in future.

Lastly, we compute averaged kinetic energy fluxes for hydrodynamic and MHD turbulence using the following flux formula^{30,40}:

$$\begin{aligned} \Pi_u(K) = & a_3 k_{K-1} \langle \Im(u_{K-1}^* u_K^* u_{K+1}^*) \rangle \\ & - a_1 k_K \langle \Im(u_K^* u_{K+1}^* u_{K+2}^*) \rangle. \end{aligned} \quad (44)$$

In Figure 5, we plot the kinetic energy fluxes for the three ϵ_{inj} . The figure clearly show that for all the three cases,

$$\Pi_{u,\text{MHD}} < \Pi_{u,\text{HD}}. \quad (45)$$

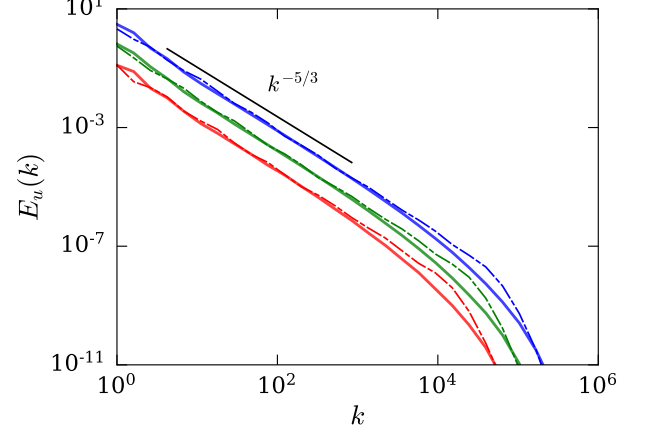


FIG. 4. (color online) Plots of kinetic energy spectra $E_u(k)$ for injection rates $\epsilon_{\text{inj}} = 0.1$ (red), $\epsilon_{\text{inj}} = 1.0$ (green), and $\epsilon_{\text{inj}} = 10.0$ (blue). The solid curves represent the $E_u(k)$ for MHD turbulence, and the dashed curves for hydrodynamic turbulence. Kolmogorov's $-5/3$ scaling (black) fits well in the inertial range for all the cases.

We also compute Π_B as $\epsilon_{\text{inj}} - \Pi_u$, and observe it to be positive. That is, the magnetic field receives energy from the velocity field. These results are consistent with the discussion of Sec. III.

The above results on $\Pi_u(K)$ are consistent with the fact that $\langle |(\mathbf{u} \cdot \nabla) \mathbf{u}| \rangle$ for MHD turbulence is lower than the corresponding term for hydrodynamic turbulence (see Table I); lower $\langle |(\mathbf{u} \cdot \nabla) \mathbf{u}| \rangle$ leads to lower kinetic energy flux. In addition, lower $\langle |(\mathbf{u} \cdot \nabla) \mathbf{u}| \rangle$ produces larger U for MHD turbulence. We also remark that the above trends on the energy fluxes are consistent with the Mininni et al.'s results²⁹ based on direct numerical simulations.

Thus, our numerical simulations demonstrate that MHD turbulence has lower $\langle |(\mathbf{u} \cdot \nabla) \mathbf{u}| \rangle$ and kinetic energy flux, but a larger U compared to hydrodynamic turbulence. These results demonstrate that turbulent drag is indeed reduced in MHD turbulence.

In the next section we will describe turbulent drag reduction in QSMHD turbulence.

V. DRAG REDUCTION IN QSMHD TURBULENCE IN TERMS OF ENERGY FLUX

Quasi-static MHD turbulence, a special class of MHD flows, has very small magnetic Prandtl number^{17,41}. A typical example of QSMHD is a liquid metal flow with a strong external magnetic field. In a nondimensionalized set of equations, the Lorentz force is proportional to $-N\mathbf{u}$, hence it is dissipative^{17,41}. The parameter N , called *interaction parameter*, is the ratio of the Lorentz

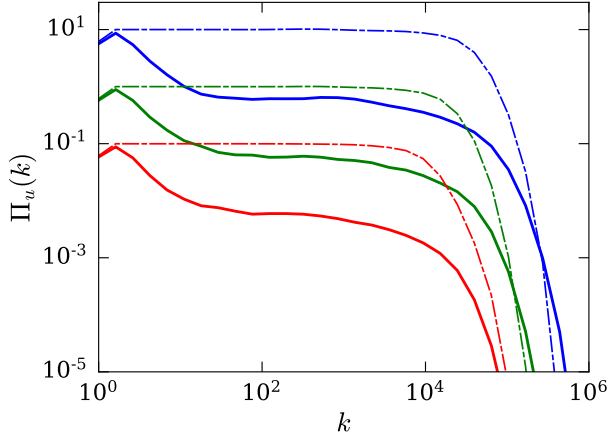


FIG. 5. (color online) Plots of kinetic energy fluxes $\Pi_u(k)$ for the different injection rates $\epsilon_{\text{inj}} = 0.1$ (red), $\epsilon_{\text{inj}} = 1.0$ (green), and $\epsilon_{\text{inj}} = 10.0$ (blue). The solid curves represent the $\Pi_u(k)$ for MHD turbulence, while the dashed curves for hydrodynamic turbulence.

force and nonlinear term $(\mathbf{u} \cdot \nabla)\mathbf{u}$, or

$$N = \frac{\sigma B_0^2 L}{\rho U}, \quad (46)$$

where σ is the electrical conductivity, and \mathbf{B}_0 is the external magnetic field, which is assumed to be constant.

In QSMHD turbulence^{17,41}, the corresponding force and related energy transfer rates are

$$\mathbf{F}_u(\mathbf{k}) = -N\mathbf{u}(\mathbf{k}) \cos^2 \theta, \quad (47)$$

$$\mathcal{F}_u(\mathbf{k}) = \Re[\mathbf{F}_u(\mathbf{k}) \cdot \mathbf{u}^*(\mathbf{k})] = -2NE_u(\mathbf{k}) \cos^2 \theta < 0, \quad (48)$$

where θ is the angle between the external magnetic field \mathbf{B}_0 and the wavenumber \mathbf{k} . Therefore, the energy transferred from the velocity field to the magnetic field, $\Pi_B(K)$, takes the following form:

$$\Pi_B(K) = - \sum_{k \leq K} \mathcal{F}_u(\mathbf{k}) = \sum_{k \leq K} 2NE_u(\mathbf{k}) \cos^2 \theta > 0. \quad (49)$$

Hence, the dissipative Lorentz force transfers the kinetic energy to the magnetic energy, which is immediately destroyed by Joule dissipation. Hence, as argued above, the kinetic energy flux is suppressed compared to the hydrodynamic turbulence.

As argued in the previous section, the depleted Π_u in QSMHD turbulence leads to a reduction in turbulent drag. Physically, the magnetic field smoothens the velocity field compared to hydrodynamic turbulence. Therefore, we expect the turbulent drag in QSMHD turbulence to be lower than the corresponding hydrodynamic counterpart.

Reddy and Verma⁴² simulated QSMHD turbulence for a wide range of interaction parameter N with a constant

TABLE II. For simulation of QSMHD turbulence by Verma and Reddy⁴³, root mean square (rms) velocity of the flow (U) as a function of interaction parameter N . The flow speed increases with the increase of N .

N	1.7	18	27	220
U	0.39	0.51	0.65	0.87

energy injection rate of 0.1 (in nondimensional unit). In Table II we list the rms velocity U as a function of N . Here, U is measured in units of L/T , where L, T are length and time scales of the large scale eddies. Clearly, U increases monotonically with N . In other words, the turbulent drag is reduced in QS MHD turbulence. It is important to note that a large U does not necessarily imply a large nonlinear term $(\mathbf{u} \cdot \nabla)\mathbf{u}$, which depends on U , as well as on the phase relations between the velocity modes. The magnetic field alters the phase relations in $(\mathbf{u} \cdot \nabla)\mathbf{u}$; thus suppresses this term and the drag; and produces larger U .

The reduced turbulent flux plays an important role in drag reduction. Note however that such reduction does not occur in laminar QSMHD because the Lorentz force damps the flow further. For example, in a QSMHD channel flow, the maximum velocity in the centre of the channel is^{17,44}

$$U_{\text{QSMHD}} = -\frac{1}{\sigma B_0^2} \left(\frac{\partial p}{\partial x} \right). \quad (50)$$

In contrast, in a hydrodynamic channel flow, the maximum velocity is⁴⁵

$$U_{\text{HD}} = -\frac{d^2}{2\nu\rho} \left(\frac{\partial p}{\partial x} \right), \quad (51)$$

where d is half-width of the channel. The ratio of the two velocities is

$$\frac{U_{\text{QSMHD}}}{U_{\text{HD}}} = \frac{2\nu\rho}{\sigma B_0^2 d^2} = \frac{1}{\text{Ha}^2}, \quad (52)$$

where Ha is the Hartmann number, which is much larger than unity for QSMHD turbulence. Hence, the velocity in laminar QSMHD is much smaller than that in hydrodynamic channel. In contrast, in a turbulent flow, the Lorentz force suppresses $\langle |(\mathbf{u} \cdot \nabla)\mathbf{u}| \rangle$, and hence increases the mean velocity. Thus, the aforementioned drag reduction is a nonlinear phenomena, which is related to the energy flux. We remark that such reduction in fluctuations have been observed in laboratory experiments. For example, Berhanu *et al.*⁴⁶ observed significant reduction in velocity fluctuations in a turbulent flow of gallium under an external magnetic field. In addition, suppression of fluctuations in QSMHD turbulence finds applications in engineering, for example, in crystal growth and plate rolling²²⁻²⁴.

In the next section, we show that a similar process is at work in turbulent flows with dilute polymers. We discuss this briefly to make a connection between turbulent drag reduction in MHD turbulence with that in a polymeric solution.

VI. REVISITING TURBULENT DRAG REDUCTION WITH DILUTE POLYMERS

Among a large body of works on turbulent drag reduction in polymers³⁻⁷, those related to the energy fluxes of polymeric flows are quite small in number. Recently, Valente *et al.*^{47,48} performed numerical simulations of polymeric solution and computed various energy fluxes. They showed a transfer of kinetic energy to the elastic energy of polymers for a set of parameters. Nguyen *et al.*⁴⁹ reported similar energy transfers, but they also showed a transfer from the elastic energy to the kinetic energy at small scales. Using numerical simulations, Benzi *et al.*⁵⁰ and Perlekar *et al.*⁵¹ analysed the energy spectra and dissipation rates of kinetic and elastic energies. Thais *et al.*⁵² computed the above quantities using turbulent stresses. Ray and Vincenzi⁵³, and Kalelkar *et al.*⁵⁴ studied the turbulent drag reduction in polymers using shell model. Several numerical simulations explore the effects of various parameters—elasticity, Reynolds number, geometry of polymers—on turbulent drag reduction^{55,56}. In this paper we relate the energy fluxes in polymeric turbulence to turbulent drag reduction.

Polymers are often described using finitely extensible nonlinear elastic-Peterlin (FENE-P) model^{2,6}. In this model, the equations for a turbulent flow with dilute polymer in tensorial form are^{2,6,57}

$$\frac{\partial u_i}{\partial t} + u_j \partial_j u_i = -\partial_i p / \rho + \nu \partial_{jj} u_i + \frac{\mu}{\tau_p} \partial_j (f w_{ij}) + F_{\text{ext},i}, \quad (53)$$

$$\frac{\partial w_{ij}}{\partial t} + u_l \partial_l w_{ij} = w_{il} \partial_l u_j + w_{jl} \partial_l u_i + \frac{1}{\tau_p} [f w_{ij} - \delta_{ij}] \quad (54)$$

$$\partial_i u_i = 0, \quad (55)$$

where ρ is the mean density of the solvent, ν is the kinematic viscosity, μ is an additional viscosity parameter, τ_p is the polymer relaxation time, and f is the renormalized Peterlin's function. In the above equations, the following forces are associated with \mathbf{u} and w_{ij} (apart from constants):

$$F_{u,i} = \partial_j (f w_{ij}), \quad (56)$$

$$F_{w,ij} = w_{il} \partial_l u_j + w_{jl} \partial_l u_i. \quad (57)$$

In Fourier space, the energy feed to kinetic energy by \mathbf{F}_u is

$$\mathcal{F}_u(\mathbf{k}) = - \sum_{\mathbf{p}} \Im [k_j f(\mathbf{q}) w_{ij}(\mathbf{p}) u_i^*(\mathbf{k})], \quad (58)$$

where $\mathbf{q} = \mathbf{k} - \mathbf{p}$. The net energy transferred from the velocity modes inside the sphere of radius K to all the modes of the polymer is

$$\Pi_w(K) = \sum_{k \leq K} -\mathcal{F}_u(\mathbf{k}). \quad (59)$$

Using numerical simulations of polymeric turbulence, Valente *et al.*^{47,48} analysed the energy transfers, in particular, the fluxes Π_u and Π_w . These fluxes depend on

the Deborah number, De , which is the ratio of the relaxation time scale of the polymer and the characteristic time scale for the energy cascade. A common feature among all the numerical runs is that $\Pi_w > 0$. In addition, the transfer from kinetic energy to elastic energy is maximum when $De \sim 1$. For example, Valente *et al.*⁴⁷ showed that for $De = 1.17$, $\Pi_w/\epsilon_{\text{inj}} \approx 0.8$ for $k\eta > 0.2$ where η is Kolmogorov's wavenumber; and $\Pi_u/\epsilon_{\text{inj}}$ peaks to approximately 0.3 near $k\eta \approx 0.1$. Thus, Π_u is reduced to around 20% to 30% for this case. We expect similar reduction for other cases when $De \sim 1$. Using a shell model, Ray and Vincenzi⁵³ showed that the kinetic energy is transferred to the polymer elastic energy. Thais *et al.*⁵², and Nguyen *et al.*⁴⁹ arrived at similar conclusions based on their direct numerical simulation of polymeric turbulence. Based on these observations, we deduce that

$$\Pi_{u,\text{Polymeric}} < \Pi_{u,\text{HD}}. \quad (60)$$

This reduction leads to a decrease in $\langle |(\mathbf{u} \cdot \nabla) \mathbf{u}| \rangle$ and in turbulent drag (also see Sec. III). Note however that in the laminar regime, the energy flux vanishes and hence the drag is not reduced. This is consistent with the observations by Sreenivasan and White⁵, and with the formulas for laminar QSMHD discussed in the previous section. It will be interesting to perform a comparative study between the shell models for polymers and hydrodynamic, as in Sec. IV.

Earlier, Fouxon and Lebedev⁵⁷ showed that the equations for dilute polymers are intimately connected to those of MHD turbulence. Hence, the aforementioned energy transfers^{47,52,53} from the kinetic energy to elastic energy is consistent with the results of MHD turbulence.

We end this section with a cautionary remark. Turbulent drag reduction in a polymer solution is attributed to many factors: boundary layers, viscoelasticity, turbulence in the bulk, interactions between polymers and large scale velocity field, anisotropy, polymer concentration, elasticity parameters, Reynolds number, etc.^{3-7,55,56} In the paper we focus on the reduction in kinetic energy flux due to polymers. More detailed and comprehensive simulations and experiments with all the above parameters are required for a definitive conclusion.

Turbulent drag reduction has also been reported in flows with bubbles (e.g. L'vov *et al.*⁸). It has been argued that kinetic energy may be transferred to the elastic energy of the bubbles; this process may be important for the turbulent drag reduction in bubbly turbulence.

We conclude in the next section.

VII. DISCUSSIONS AND CONCLUSIONS

In this paper we show that MHD turbulence and quasi-static MHD (QSMHD) turbulence exhibit turbulent drag reduction. We relate the above to the reduced kinetic energy flux due to a partial transfer of kinetic energy flux to the magnetic field. This process leads to a suppression

of the nonlinear term $\langle |(\mathbf{u} \cdot \nabla) \mathbf{u}| \rangle$, and stronger rms velocity U compared to hydrodynamic turbulence. Similar reduction in kinetic energy flux has been reported in solutions with dilute polymers and bubbles. Thus, the energy flux provides a useful perspective on turbulent drag reduction. We remark that some of the works by Eyink et al.^{58,59} and Jafari et al.^{60–62} are useful in quantifying randomness in hydrodynamic and MHD turbulence. These authors also studied stochasticity in dynamo.

We simulated shell models of hydrodynamic and MHD turbulence, and computed the rms velocities, $\langle |(\mathbf{u} \cdot \nabla) \mathbf{u}| \rangle$, and kinetic energy fluxes for the two cases. For the same kinetic energy injection rate, $\langle |(\mathbf{u} \cdot \nabla) \mathbf{u}| \rangle$ and kinetic energy flux in MHD turbulence are lower than those for hydrodynamic turbulence. However, the rms velocity is larger for MHD turbulence; this enhanced velocity still yields suppression in $\langle |(\mathbf{u} \cdot \nabla) \mathbf{u}| \rangle$ in MHD turbulence due to the phase relations of the complex Fourier modes. Our simulations also show that in MHD turbulence, a finite amount of energy is transferred from the velocity field to the magnetic field. These numerical observations demonstrate turbulence drag reduction in MHD turbulence. Direct numerical simulations of hydrodynamic and MHD turbulence will provide stronger credence to the above theory. However, such simulations are very expensive, and they are planned for future.

Turbulent drag reduction in MHD turbulence has important ramifications in astrophysical and engineering flows. We believe that this feature would have consequences in solar and planetary dynamos. In a subcritical dynamo transition, a finite magnetic field appears at one transition point, and a finite magnetic field shut-down abruptly at the other transition point^{33,63}. When we carry forward our results discussed in this paper to such a system, we expect that the generated magnetic field would suppress the nonlinear term $\langle |(\mathbf{u} \cdot \nabla) \mathbf{u}| \rangle$ and enhance U , while shutdown of the dynamo would enhance $\langle |(\mathbf{u} \cdot \nabla) \mathbf{u}| \rangle$ and suppress U . Yadav *et al.*³³ observed precisely this feature in their simulation of subcritical dynamo transition with small magnetic Prandtl number. We can relate this result to the Martian dynamo. At present, Mars has no magnetic field, but there are evidences of strong crustal magnetic field. Hence, researchers believe that dynamo action was present in Mars in the past, but it got shutdown via a subcritical dynamo transition⁶⁴. Based on the above arguments, we can conjecture that during this dynamo shutdown, $\langle |(\mathbf{u} \cdot \nabla) \mathbf{u}| \rangle$ may have increased, while the mean U may have been weakened. We hope that numerical simulations may verify this conjecture.

In addition, we expect that our findings would be useful for understanding the dynamics of some of the laboratory dynamos employed to understand geodynamo⁶⁵. Note that the large laboratory devices for studying dynamo transitions need to be robust enough to handle the aforementioned sudden increase in the large-scale velocity field. These issues would be of concern to the designers of the experiments. In addition, the magnetic field

can be used to suppress fluctuations or the nonlinear term $\mathbf{u} \cdot \nabla \mathbf{u}$ in engineering flows, as in crystal growth and plate rolling^{22–24}. These ideas help in producing smooth plates for aerodynamic designs and defect-free large crystals.

Turbulent drag reduction for aircrafts and automobiles is an interesting and challenging problem. Towards this objective, researchers have devised many interesting schemes including laminar flow control, control of boundary layer detachment, injection of travelling waves, etc.^{66,67} This phenomena is related to the relaminarization of fluid flows. Narasimha and Sreenivasan⁶⁸ studied relaminarization in stably stratified turbulence, rotating turbulence, and accelerated flows, and connected relaminarization to the reduction in the nonlinear term $\langle |(\mathbf{u} \cdot \nabla) \mathbf{u}| \rangle$. Connecting the above phenomena to the energy flux would be an interesting and useful exercise.

In summary, turbulent energy flux provides valuable insights into the dynamics of drag reduction.

ACKNOWLEDGMENTS

The authors thank Abhishek Kumar, Franck Plunian, K. R. Sreenivasan, Shashwat Bhattacharya, and Supratik Banerjee for useful discussions. Soumyadeep Chatterjee is supported by INSPIRE fellowship (IF180094) of Department of Science & Technology, India.

- ¹P. A. Davidson, *Turbulence: An Introduction for Scientists and Engineers* (Oxford University Press, Oxford, 2004).
- ²P. Sagaut and C. Cambon, *Homogeneous turbulence dynamics*, 2nd ed. (Cambridge University Press, Cambridge, 2018).
- ³M. Tabor and P. G. de Gennes, EPL **2**, 519 (1986).
- ⁴P. G. de Gennes, *Introduction to Polymer Dynamics* (Cambridge University Press, Cambridge, 1990).
- ⁵K. R. Sreenivasan and C. M. White, J. Fluid Mech. **409**, 149 (2000).
- ⁶R. Benzi, Physica D **239**, 1338 (2010).
- ⁷R. Benzi and E. S. C. Ching, Annu. Rev. Condens. Matter Phys. **9**, 163 (2018).
- ⁸V. S. L'vov, A. Pomyalov, I. Procaccia, and V. Tiberkevich, Phys. Rev. Lett. **94**, 315 (2005).
- ⁹A. N. Kolmogorov, Dokl Acad Nauk SSSR **32**, 16 (1941).
- ¹⁰A. N. Kolmogorov, Dokl Acad Nauk SSSR **30**, 301 (1941).
- ¹¹T. G. Cowling, *Magnetohydrodynamics* (Adam Hilger, London, 1976).
- ¹²G. Dar, M. K. Verma, and V. Eswaran, Physica D **157**, 207 (2001).
- ¹³A. Alexakis, P. D. Mininni, and A. G. Pouquet, Phys. Rev. E **72**, 046301 (2005).
- ¹⁴P. D. Mininni, A. Alexakis, and A. G. Pouquet, Phys. Rev. E **72**, 046302 (2005).
- ¹⁵O. Debligny, M. K. Verma, and D. Carati, Phys. Plasmas **12**, 042309 (2005).
- ¹⁶R. Kumar, M. K. Verma, and R. Samtaney, EPL **104**, 54001 (2014).
- ¹⁷M. K. Verma, Rep. Prog. Phys. **80**, 087001 (2017).
- ¹⁸A. Alexakis and L. Biferale, Phys. Rep. **767–769**, 1 (2018).
- ¹⁹L. Onsager, Il Nuovo Cimento **6**, 279 (1949).
- ²⁰G. L. Eyink and K. R. Sreenivasan, Rev. Mod. Phys. **78**, 87 (2006).
- ²¹G. L. Eyink, arXiv.org, arXiv:1803.02223 (2018).
- ²²A. Bojarevics, Y. M. Gel'fgat, and L. A. Gorbunov, in *Liquid Metal Magnetohydrodynamics*, edited by J. J. Lielpeteris and R. J. Moreau (Kluwer Academic Publishers, 1989) pp. 127–133.

- ²³E. P. Bochkarev, V. M. Foliforov, J. M. Gelfgat, L. A. Gorbunov, V. S. Gorovic, O. V. Pelevin, and G. N. Petrov, in *Liquid Metal Magnetohydrodynamics*, edited by J. J. Lielpeteris and R. J. Moreau (Kluwer Academic Publishers, 1989) pp. 135–143.
- ²⁴A. J. Chudinovskij, S. B. Dement'ev, E. V. Shcherbinin, V. K. Vlasjuk, and L. A. Volokhonskij, in *Liquid Metal Magnetohydrodynamics*, edited by J. J. Lielpeteris and R. J. Moreau (Kluwer Academic Publishers, 1989) pp. 187–193.
- ²⁵U. Frisch, *Turbulence: The Legacy of A. N. Kolmogorov* (Cambridge University Press, Cambridge, 1995).
- ²⁶R. H. Kraichnan, and A. G. Pouquet, *ApJ* **626**, 853 (2005).
- ²⁷M. K. Verma, *Phys. Rep.* **401**, 229 (2004).
- ²⁸M. K. Verma, *Physics of Buoyant Flows: From Instabilities to Turbulence* (World Scientific, Singapore, 2018).
- ²⁹P. D. Mininni, Y. Ponty, D. C. Montgomery, J.-F. Pinton, H. Politano, and A. G. Pouquet, *ApJ* **626**, 853 (2005).
- ³⁰M. K. Verma and R. Kumar, *J. Turbul.* **17**, 1112 (2016).
- ³¹H. K. Moffatt, *Magnetic Field Generation in Electrically Conducting Fluids* (Cambridge University Press, Cambridge, 1978).
- ³²R. Monchaux, M. Berhanu, S. Aumaitre, A. Chiffaudel, F. Daviaud, B. Dubrulle, F. Ravelet, S. Fauve, N. Mordant, F. Petrelis, M. Bourgoin, P. Odier, J.-F. Pinton, N. Plihon, and R. Volk, *Phys. Fluids* **21**, 035108 (2009).
- ³³R. K. Yadav, M. K. Verma, and P. Wahi, *Phys. Rev. E* **85**, 036301 (2012).
- ³⁴M. Yamada and K. Ohkitani, *Phys. Rev. E* **57**, R6257 (1998).
- ³⁵E. B. Gledzer, *Dokl Acad Nauk SSSR* **209**, 1046 (1973).
- ³⁶V. S. L'vov, E. Podivilov, A. Pomyalov, I. Procaccia, and D. Vandembroucq, *Phys. Rev. E* **58**, 1811 (1998).
- ³⁷P. Frick and D. D. Sokoloff, *Phys. Rev. E* **57**, 4155 (1998).
- ³⁸R. Stepanov and F. Plunian, *J. Turbul.* **7**, 1 (2006).
- ³⁹F. Plunian, R. Stepanov, and P. Frick, *Phys. Rep.* **523**, 1 (2012).
- ⁴⁰M. K. Verma, *Energy transfers in Fluid Flows: Multiscale and Spectral Perspectives* (Cambridge University Press, Cambridge, 2019).
- ⁴¹B. Knaepen and R. Moreau, *Annu. Rev. Fluid Mech.* **40**, 25 (2008).
- ⁴²K. S. Reddy and M. K. Verma, *Phys. Fluids* **26**, 025109 (2014).
- ⁴³M. K. Verma and K. S. Reddy, *Phys. Fluids* **27**, 025114 (2015).
- ⁴⁴U. Müller and L. Bühler, *Magnetofluidynamics in Channels and Containers* (Springer-Verlag, Berlin Heidelberg, 2001).
- ⁴⁵P. K. Kundu, I. M. Cohen, and D. R. Dowling, *Fluid Mechanics*, 6th ed. (Academic Press, San Diego, 2015).
- ⁴⁶M. Berhanu, B. Gallet, N. Mordant, and S. Fauve, *Phys. Rev. E* **78**, 015302 (2008).
- ⁴⁷P. C. Valente, C. B. da Silva, and F. T. Pinho, *J. Fluid Mech.* **760**, 39 (2014).
- ⁴⁸P. C. Valente, C. B. da Silva, and F. T. Pinho, *Phys. Fluids* **28**, 075108 (2016).
- ⁴⁹M. Q. Nguyen, A. Delache, S. Simoëns, W. J. T. Bos, and M. El Hajem, *Phys. Rev. Fluids* **1**, 083301 (2016).
- ⁵⁰R. Benzi, E. De Angelis, R. Govindarajan, and I. Procaccia, *Phys. Rev. E* **68**, 016308 (2003).
- ⁵¹P. Perlekar, D. Mitra, and R. Pandit, *Phys. Rev. Lett.* **97**, 264501 (2006).
- ⁵²L. Thais, T. B. Gatski, and G. Mompean, *Int. J. Heat Mass Transfer* **43**, 52 (2013).
- ⁵³S. S. Ray and D. Vincenzi, *EPL* **114**, 44001 (2016).
- ⁵⁴C. Kalelkar, R. Govindarajan, and R. Pandit, *Phys. Rev. E* **72**, 017301 (2005).
- ⁵⁵G. Boffetta, A. Celani, and A. Mazzino, *Phys. Rev. E* **71**, 036307 (2005).
- ⁵⁶R. Benzi, E. S. C. Ching, E. De Angelis, and I. Procaccia, *Phys. Rev. E* **77**, 046309 (2008).
- ⁵⁷A. Fouxon and V. Lebedev, *Phys. Fluids* **15**, 2060 (2003).
- ⁵⁸G. L. Eyink, A. Lazarian, and E. T. Vishniac, *The Astrophysical Journal* **743**, 51 (2011).
- ⁵⁹G. L. Eyink, E. Vishniac, C. Lalescu, H. Aluie, K. Kanov, K. Bürger, R. Burns, C. Meneveau, and A. Szalay, *Nature* **497**, 466 (2013).
- ⁶⁰A. Jafari and E. Vishniac, *Phys. Rev. E* **100**, 013201 (2019).
- ⁶¹A. Jafari, E. Vishniac, and V. Vaikundaraman, *Phys. Rev. E* **100**, 043205 (2019).
- ⁶²A. Jafari, E. Vishniac, and V. Vaikundaraman, *Phys. Rev. E* **101**, 022122 (2020).
- ⁶³M. K. Verma and R. K. Yadav, *Phys. Plasmas* **20**, 072307 (2013).
- ⁶⁴W. J. Kuang, W. Jiang, and T. Wang, *Geophys. Res. Lett.* **35**, L14204 (2008).
- ⁶⁵D. P. Lathrop and C. B. Forest, *Phys. Today* **64**, 40 (2011).
- ⁶⁶D. M. Bushnell, *Proc. Instn. Mech. Engrs.* **217**, 1 (2003).
- ⁶⁷H. Mamori, K. Iwamoto, and A. Murata, *Phys. Fluids* **26**, 015101 (2014).
- ⁶⁸R. Narasimha and K. R. Sreenivasan, *Adv. Appl. Mech.* **19**, 221 (1979).